PAPER

Impact of generalized heat and mass flux models on Darcy–Forchheimer Williamson nanofluid flow with variable viscosity

IOP Publishing Physica Scripta
Phys. Scr. 94 (2019) 125201 (11pp) https://doi.org/10.1088/1402-4896/ab2e7e

Impact of generalized heat and mass flux models on Darcy–Forchheimer Williamson nanofluid flow with variable viscosity

T Salahuddin, Shah Muhammad and Sana Sakinder

Mirpur University of Science and Technology (MUST), Mirpur 10250 (AJK), Pakistan

E-mail: taimoor.maths@must.edu.pk

Received 26 June 2019
Accepted for publication 2 July 2019
Published 5 September 2019

Abstract

In the current study, we analyze the 2D Williamson nanoliquid flow due to variable thickness surface embedded in permeable space. Cattaneo–Christov heat and mass flux assumptions have been employed for the embodiment of heat and mass equations. Flow is generated by an exponential stretchable sheet. The Darcy–Forchheimer model is considered to scrutinize the liquid flow in a porous medium. The case of prescribed exponential surface temperature of heat transfer is examined. A model is contrived to comprise the partial differential equations and then transform them into ordinary differential equations by imposing an appropriate non-dimensional similarity transformation. The bvp4c technique is used to execute the laborious non-linear equations. A numerical interpretation is manifested to incorporate the skin friction values. The significance of the effect on the involved parameters is presented in graphs and discussed in detail.

Keywords: fluid, fluid flow, heat transfer

(Some figures may appear in colour only in the online journal)

Introduction

In 1929 Williamson [1] explicated the flow of pseudoplastic liquids and presented a model to explain the flow of pseudoplastic liquids and empirically established the resultant role. Williamson liquid is a type of pseudoplastic fluid having the nature of shear thinning. Pseudoplastic fluids are mostly found in non-Newtonian fluids. Many investigators have studied the boundary layer flow of pseudoplastic fluids as it has extensive relevance in many fields such as geophysics, biological sciences and the petroleum industry. This type of flow extensively occurs in the emulsion of coated sheets, food processing, polymer processing, extrusion of polymer sheets, plastic manufacturing and various other processes. The rheological characteristics of fluid cannot be deliberated through the Navier–Stokes equation alone. Blood is assumed to be behave like Williamson fluid, which is why much attention has been paid to it by many researchers. The Williamson parameter is the relation of the relaxation to the retardation time, where relaxation time refers to the time taken by the liquid to return from a deformed state to its initial state. The time needed to rectify the applied force is retardation. Malik *et al* [2] explored the numerical interpretation for the magnetohydrodynamic (MHD) stagnation point of Williamson liquid over a stretchable cylinder in the neighborhood of the stagnation point. Ariel *et al* [3] examined the extended homotopy for laminar flow over an extending sheet. Akbar *et al* [4] retrieved the numerical and analytic results of peristaltic flow of Williamson fluid. The peristaltic flow of the Williamson model in a asymmetrical channel was elucidated by Nadeem *et al* [5]. Scarpi and Dapara [6] established a perturbation method for Williamson fluid interjected into rock rupture.

There are several cases in chemical engineering, environmental, geophysical and industrial systems involving flow transport through a porous medium. Flow subject to a porous medium has extrusive applications; such applications may comprise the movement of water in reservoirs, gas cleaning filtration, insulation of granules and fiber, blood flow through arteries, oil production, catalytic reactors, the fermentation process and numerous others. It is clear from the literature that classical Darcy law has attracted the interest of many scientists due to its distinctive use in the field of science. The phenomenon of Darcy law has been widely used in order to

execute the flow of drenched permeable media. The main drawback of Darcian expression is that it is faintly copious under the circumstances of weaker porosity and lower velocity. The difficulty emerges when exceeding the Reynold's number, and the nature of the flow assimilates to a non-linear flow, in which the substantial effects of inertial and boundary demand the extension of non-Darcian expression. There are many substantial experiments that involve a higher inertial and boundary effect at a higher flow rate. In such conditions, Darcy law fails to characterize the behavior of flow as laminar, turbulent or transient. Eventually, in 1901, the Dutch scientist Forchheimer [7] prolonged the quadratic velocity expression for the prognosis of the effect of boundary and inertial flow. Essentially dominant filtration velocities generate quadratic stress for a permeable medium in the momentum expression. Muskat [8] named this term as 'Forchheimer' and verified that non-Darcian expression is also cogent for an extreme Reynold's number. Mondal and Pal [9] validated the hydromagnetic convective diffusion of species in the Darcy–Forchheimer model past an exponential space and concluded that solutal distribution dwindles when increasing the electric field parameter. Hakeem and Ganesh [10] accounted for the Darcy–Forchheimer MHD nanoliquid flow with thermally layered permeable space past an exponential extending sheet. Sing *et al* [11] incorporated the Darcy–Forchheimer model and studied the characteristics of Brinkman fluid flow with heat transfer. The Darcy–Forchheimer model for magneto-Maxwell fluid instigated by convective heat surface was studied by Sadiq and Hayyat [12].

The typical type of common base liquids, essentially ethylene glycol, engine oil and water, have inadequate characteristics of low thermal conductivity. They do not meet the required standard for use in prevalent industrial applications. Conventional fluids have remarkable thermal conductivity. The concept of new nano-technology was proposed by Choi [13]. Nanofluids have extensive applications in the fields of solar cells, refrigerators, computer chips, ceramic industry, grinding machines, car engines, etc. A nanoliquid is a homogeneous solution of base liquid and nanoparticles. Nanoliquids remarkably transmute the performance of base liquids which modify the thermal conductivity, density, viscosity, etc. In 2006, Buongiorno [14] ascertained that the first two models proposed in the previous literature have the limitation that nanoparticles do not accelerate with fluid streamlines in a passive manner. Considerable efforts were made by researchers to execute the eccentric strength in the viscosity and thermal conductivity of nanoliquids. Seven slip components (Magnus effect, gravity, thermophoresis, inertia, Brownian diffusion, diffusiophoresis and drainage) were instigated by Buongiorno that can produce a relative velocity between the base liquid and nanoparticles. He evaluated all of the seven impacts and concluded that the eccentric accretion in the thermal conductivity is the consequence of thermophoresis and Brownian movement. Kuznetsov and Nield [15] inspected a tangible existent case of the boundary layer which explored the signification of Brownian diffusion and thermophoresis. Mustafa *et al* [16] investigated the boundary layer flow of nanoliquid past a non-linear stretchable sheet with convective boundary condition. Eastman *et al* [17] reported copper nanoparticles in ethylene glycol and produced the result that the shape of nanoparticles has a robust impact on thermal conductivity. The impact of Lorentz force around the stagnation point on tangent hyperbolic fluid was contemplated by Salahuddin *et al* [18]. Rehman [19] considered the Buongiornio model and revealed the properties of force convective flow and heat transfer in a penetrable stretchable plate in the presence of second-order slip conditions at the interface. Solar radiation impacts and thermal generation in Carreu fluid with variable thickness were explored by Khan *et al* [20].

The heat transport mechanism occurs between two distant kinds of objects or temperature differences between distinctive parts of a similar system. The heat transfer mechanism has attracted the attention of many scientists due to its prodigious applications such as power generation, nuclear reactors, pharmaceuticals, the petroleum industry, crystal growth distillation columns and numerous others. In the past few decades, investigators have employed the renowned Fourier's [21] law of heat induction, while Fick's [22] law is usually intimated for the essential aspects of mass transfer as previous literature shows. The animalistic behavior of the concentration and temperature diffusions are ignored in Fourier's and Fick's laws. The major inability of Fourier's and Fick's laws is that concentration and temperature distributions have parabolic expressions. The considerable impediment of the parabolic equation was that initial intrusion is observed completely in an entire system. This behavior is unrealistic because it controverts the 'principal of causality' which is recognized by the contradiction of heat conduction. Cattaneo [23] assumed relaxation time by considering the relaxation time, and prolonged Fourier's law. The relaxation time along with Fourier's law is sufficient to maintain the transformation of heat throughout the propagation of temperature waves with average speed. The Cattaneo equations result in hyperbolic energy equations but still, Cattaneo law is incompetent to explicate the entire behavior of heat transfer because different materials retain distinct relaxation times. By including the characteristics of temperature relaxation time, Christov [24] modified Cattaneo's law and acclimated the time derivative to preserve the material invariant expression. Thermal conductivity in a horizontal layer of viscous liquid was examined by Straughan [25] by employing the Cattaneo–Christov theory. Burgers fluid flow under the influence of thermal conductivity was explored by Waqas *et al* [26] by considering the Cattaneo–Christov model. The Cattaneo–Christov theory was incorporated by Han *et al* [27], who perceived the flow of Maxwell stretched material. Viscous nanoliquid flow past a bidirectional linearly stretchable sheet under the impact of the Cattaneo–Christov theory double diffusion was explored by Hayat *et al* [28]. Heat transfer of a rotating flow of Maxwell liquid along with the Cattaneo–Christov heat flux theory was investigated by Mustafa [29]. Khan *et al* [30] accomplished the numerical epitome for Maxwell fluid instigated by an exponentially stretching sheet by monopolizing the relaxation time. For an incompressible liquid, the existence of the Cattaneo–Christov model was accomplished by Zampoli and Tibullo [31]. Lie *et al* [32] elucidated the impact of the Cattaneo–Christov

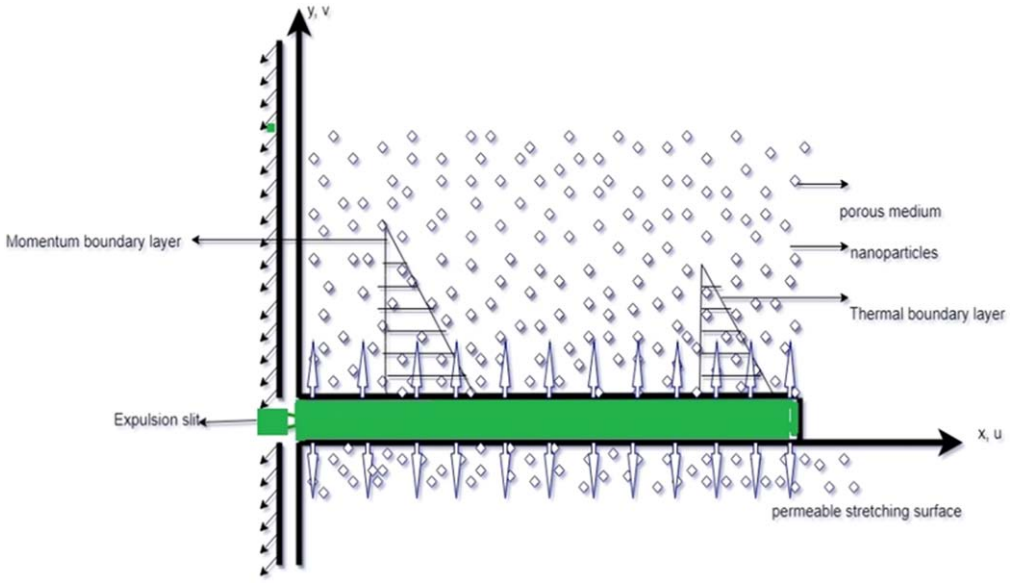

Figure 1. Geometry of the model in 2D.

model for Maxwell hydromagnetic liquid instigated by a vertically moving surface. With the appearance of the Cattaneo–Christov heat and mass flux models, the characteristics of Jeffrey fluid were scrutinized by Hayat *et al* [33].

Viscosity is a substantial feature of liquids, i.e. liquid opposition to flow, which relies upon intermolecular forces and pressure. When fluid is heated, the fluid viscosity decreases continuously. Through precise elucidation, it has been confirmed that the temperature of gases and the viscosity are directly related to one another, and inversely related in the case of fluids. The boundary layer flow for a viscous fluid enclosed by an extending sheet with variable viscosity was perceived by Fand *et al* [34]. The flow of Maxwell liquid past a stretchable sheet with variable thickness was elucidated by Hayat *et al* [35]. Flow over a continuously non-linear extending sheet with variable viscosity was investigated by Khadar *et al* [36].

The essential objective of the current work is to determine the significance of nanoparticles in 2D Williamson fluid flow confined by an extending sheet with Darcy–Forchheimer permeable media. The characteristics of thermophoresis and Brownian diffusion are also studied. The influence of Cattaneo–Christov heat and mass flux models are also considered. By appropriate consideration of the initial condition, the resultant equations are manipulated numerically by considering the algorithmic program bvp4c. The distinct involved parameters are tabularized through a benchmark and graphically to prognosticate the importance of the various parameters on velocity, thermal and solutal profiles.

Mathematical formulation

We devise a steady, 2D boundary layer flow of an incompressible Williamson nanoliquid with variable thickness drenched in permeable space explicated through the Darcy–Forchheimer model (as shown in figure 1). The heat and mass transfer mechanism is evaluated by employing the Cattaneo–Christov heat and mass flux theories. We presume that the stretching sheet is shrunk in its own axis with velocity $U_w = \sigma_0 \exp(x/L)$ and $y = 0$ is normal to the sheet.

Cauchy stress tensor for Williamson fluid model is delineated as

$$S = -pI + \tau, \tag{1}$$

$$\tau = \left(\Lambda_\infty + \frac{\Lambda_0 - \Lambda_\infty}{1 - \Gamma\dot{\eta}}\right)B_1, \tag{2}$$

where Λ_∞ is the limiting viscosity at an infinite shear rate and Λ_0 is the limiting viscosity at zero shear rate. B_1 is the first Rivlin–Ericksen tensor and $\dot{\eta}$ is delimited as

$$\dot{\eta} = \sqrt{\frac{1}{2}\pi}. \tag{3}$$

Here, we examine $\Lambda_\infty = 0, \dot{\eta} < 1$.

$$\tau = \Lambda_0(1 + \Gamma\dot{\eta})B_1. \tag{4}$$

For $\dot{\eta} = 0$, Williamson fluid becomes a regular Newtonian fluid.

We assumed a no-slip boundary condition. Here we also presumed that the extended sheet was permeable. On the wall $v = -\xi(x)$ is the suction/injection velocity. Under the aforementioned specified assumptions, the constitutive equations are

$$u_x + u_y = 0\,, \tag{5}$$

$$uu_x + vu_y = \frac{1}{\rho}[u_y\mu_y\,(T) + \mu(T)u_{yy} + \Gamma\sqrt{2}[u_y\mu_y\,(T) + \mu(T)u_{yy}]u_y] - \nu(u/K) - \delta u^2, \tag{6}$$

where K is the intrinsic permeability, ρ is the liquid density, μ is the dynamic viscosity, $\delta = \beta_e/(x\sqrt{K}$ is the inertia coefficient of the porous medium and β_e is the drag coefficient.

The advanced heat conduction and mass diffusion equations together with the thermal and solutal relaxation time can be deduced as

$$q_1 + \lambda_e(q_{1t} - q_1.\nabla v + v.\nabla q_1 + (\nabla.v)q_1) = -k_f \nabla T, \quad (7)$$

$$j_1 + \lambda_c(j_{1t} - j_1.\nabla v + v.\nabla j_1 + (\nabla.v)j_1) = -D_B \nabla C, \quad (8)$$

where j_1, q_1, v, λ_c, λ_e and D_B represent the mass flux, heat flux, velocity vector, relaxation time of mass and heat flux and Brownian diffusion coefficient. Setting the condition $\lambda_c = \lambda_e = 0$, the preceding equations turn into classical Fourier's and Fick's laws. By establishing $\nabla.V = 0$, $q_{1t} = j_{1t} = 0$ we get the following thermal and solutal equations:

$$q_1 + \lambda_e(v.\nabla q_1 - q_1.\nabla v) = -k_f \nabla T, \quad (9)$$

$$j_1 + \lambda_c(v.\nabla j_1 - j.\nabla v) = -D_B \nabla C. \quad (10)$$

Eliminating q_1 and j_1 from equations (9) and (10),

$$uT_x + vT_y + \lambda_e(u^2T_{xx} + v^2T_{yy} + uv_xT_y + vv_yT_y + 2uvT_{xy} + uu_xT_x + vu_yT_x = \alpha T_{yy} + \frac{(\rho c)_p}{(\rho c)_f}\left(D_BT_yC_y + \frac{D_T}{T_\infty}T^2{}_y\right), \quad (11)$$

$$uC_x + vC_y + \lambda_c(u^2C_{xx} + v^2C_{yy} + uv_xC_y + vv_yC_y + 2uvC_{xy} + uu_xC_x + vu_yC_x = D_BC_{yy} + \frac{D_T}{T_\infty}C_{yy}. \quad (12)$$

To transform the non-linear partial differential equations into ordinary differential equations, we introduce these suitable similarity transformations [37]:

$$u = \sigma_0 \exp(x/L)\, g'(\psi),$$
$$v = -\sqrt{\frac{(\nu\sigma_0}{2L}} \exp(x/(2L)(g(\psi) + \psi g'(\psi)),$$
$$\psi = \sqrt{\frac{\sigma_0}{2\nu L}} \exp\left(\frac{x}{(2L)}y\right). \quad (13)$$

In case of prescribed exponential surface temperature, $T = T_0 \exp(x/(2L)\theta(\psi) + T_\infty$,

$$C = C_0 \exp(x/(2L)\varphi(\psi) + C_\infty. \quad (14)$$

The governing equations yield the following form:

$$\left(1 + \frac{\lambda g''}{2}\right)\left(1 + \frac{\theta}{\theta_r}\right)g''' - \frac{\theta'}{\theta_r}\left(1 + \frac{\lambda g''}{2}\right)g'' - \gamma\left(1 + \frac{\theta}{\theta_r}\right)g' - 2F_rg'^2 - 2g'^2 - gg'' = 0, \quad (15)$$

$$(Pr\delta_c g^2 - 1)\theta'' + Pr(\theta g' - g\theta' + \delta_c(3g'^2\theta - 3\theta' gg' + \theta gg'')) - PrN_B\varphi'\theta' - Pr\theta'^2N_T = 0, \quad (16)$$

$$(Sc\delta_c g^2 - 1)N_B\varphi'' + ScN_B(\varphi g' - g\varphi' + \delta_c \times (3g'^2\varphi - 3g'g\varphi' + gg''\varphi)) - \theta''N_T = 0, \quad (17)$$

and the relevant boundary conditions are

$$g(0) = -s,\ g'(0) = 1,\ \theta(0) = 1,\ \varphi'(0) = 1,$$
$$g'(\infty) \to 0,\ \theta(\infty) \to 0\ \varphi(\infty) \to 0. \quad (18)$$

Here s indicates the injection/suction parameter, λ is the Williamson parameter, γ is the local porosity parameter, F_r is the Forchheimer parameter, Pr is the Prandtl number, N_B is the Brownian movement parameter, δ_c is the thermal relaxation time parameter, N_T is the thermophoresis parameter, δ_c is the concentration relaxation time parameter and Sc is the Schmidt number. The miscellaneous dimensionless parameters appearing in equations (15) to (17) are

$$s = -\frac{\xi(x)\sqrt{\frac{2L}{\nu\sigma_0}\exp\left(\frac{-x}{2L}\right)}}{2L},\ \lambda = \Gamma\sqrt{\frac{\sigma_0{}^3\exp(3x)/L)}{\nu L}},$$
$$\gamma = \frac{L\,\nu\exp(-x)/L)}{K\,\sigma_0},$$
$$F_r = \frac{L\,\beta_e}{x\,\sqrt{K}},\ Pr = \frac{\nu}{\alpha},\ N_B = \frac{\tau\,D_BC_0}{\nu},\ N_T = \frac{\tau\,D_TT_0}{T_\infty\nu},$$
$$\delta_e = \frac{\lambda_e\sigma_0}{L},\ \delta_c = \frac{\lambda_c\sigma_0}{L},\ Sc = \frac{\nu}{D_B}.$$

The skin friction coefficient is formalized as

$$C_g = \frac{\tau_w}{\rho U^2{}_w}\Big|_{y=0},$$

and in dimensionless form the skin friction coefficient is

$$\sqrt{(2\,\mathrm{Re}\,C_g)} = [g'' + (\lambda/2)g''^2]\left(1 - \frac{\theta}{\theta_r}\right)^{-1}, \quad (19)$$

where $Re = \sqrt{\frac{L\sigma_0\exp\left(\frac{x}{L}\right)}{\nu}}$.

Conclusion and analysis

This section is presented to clarify the interpretation of distinct engrossed parameters relative to the velocity profile $g'(\psi)$, temperature distribution $\theta(\psi)$ and solutal profile $\varphi(\psi)$. Figure 2 shows that the momentum layer thickness and velocity distribution decrease with a rise in the suction parameter while they increase for the injection case. The reason behind this phenomenon is that when fluid is inserted into the extending surface it covers the area closer to the wall which yields an increment in the momentum layer thickness. The reason for suction, however, is that liquid movement is in the outward direction from the area obstructed by the wall, which makes it difficult for the boundary layer to stabilize. Figure 3 demonstrates that increasing the Williamson parameter λ yields a minor decrease in the velocity field and boundary layer thickness. The relaxation time is also extended by increasing the Williamson parameter λ, which shows that liquid requires more resistance to flow; thus, viscous forces become further pre-eminent to the motion of liquid and the velocity decreases slightly. Figure 4 illuminates the behavior of the Forchheimer parameter F_r on the velocity profile. By enlarging F_r, a decay occurs in the velocity distribution and related momentum layer thickness. This means the boundary layer becomes thicker and therefore the liquid cannot move freely. Figure 5 shows that the porosity parameter

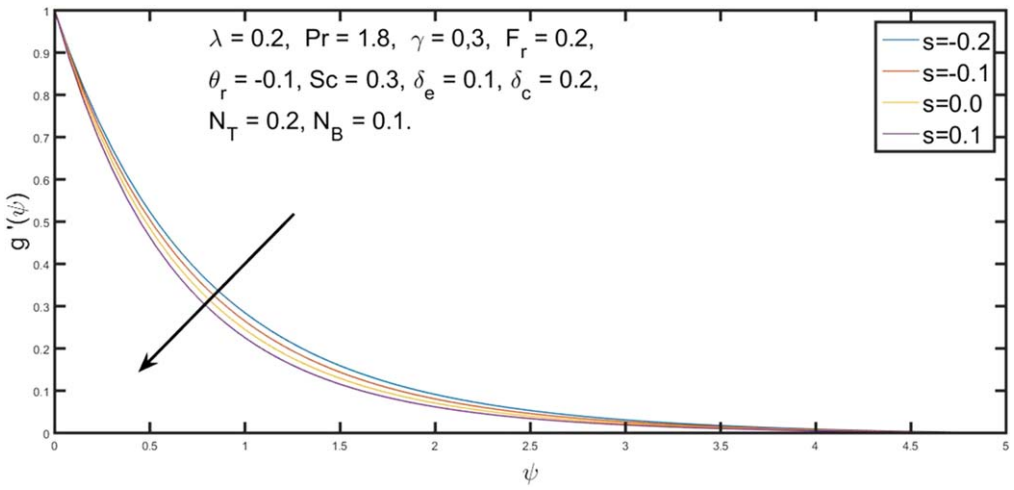

Figure 2. Effect of s on $g'(\psi)$.

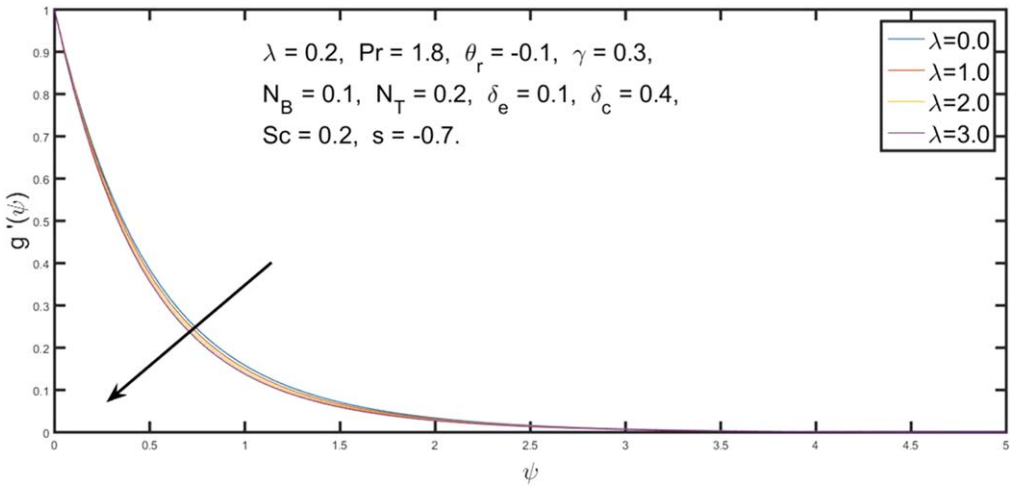

Figure 3. Effect of λ on $g'(\psi)$.

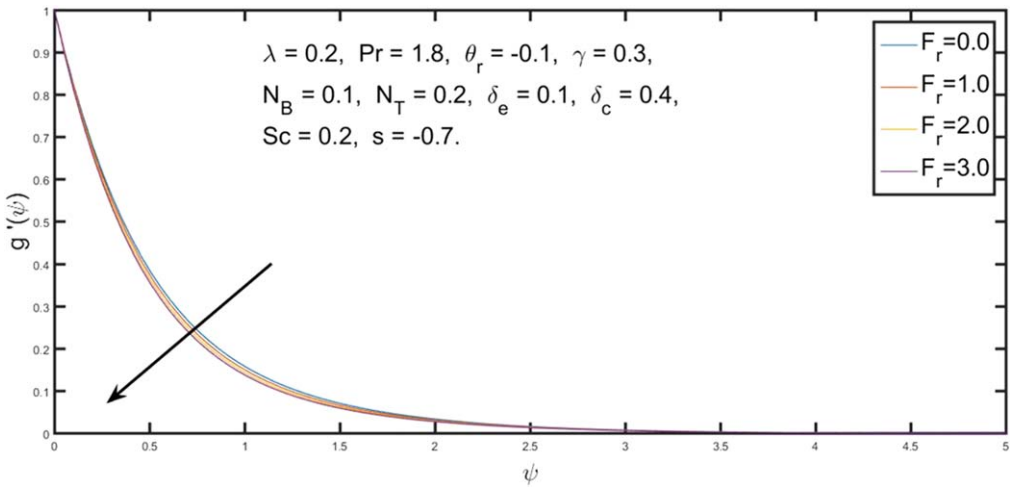

Figure 4. Effect of F_r on $g'(\psi)$.

γ has a slight impact on the velocity distribution. It reveals that extreme values of γ cause a decrease in the velocity profile. The persistence of permeable media proceeds to inflate the opposition to liquid which causes a decay in liquid velocity and associated momentum layer thickness. Figure 6 demonstrates that the velocity distribution is influenced by the variable thickness of θ_r. It is observed that the liquid velocity dwindles by raising the temperature parameter. Significantly, the liquid

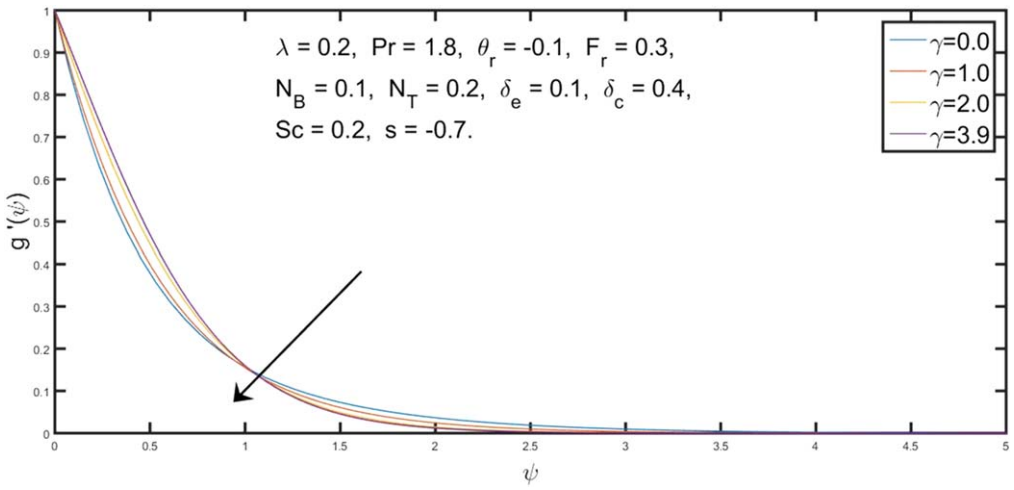

Figure 5. Effect of γ on $g'(\psi)$.

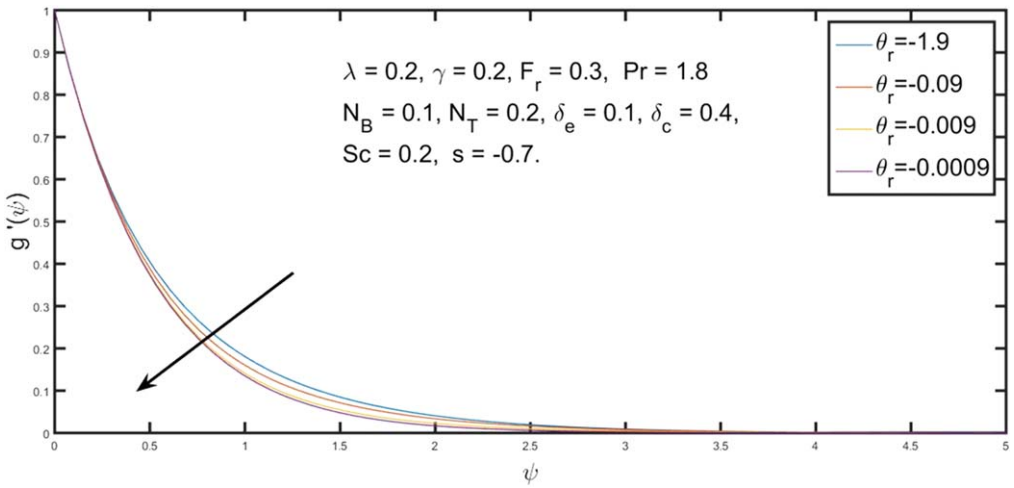

Figure 6. Effect of θ_r on $g'(\psi)$.

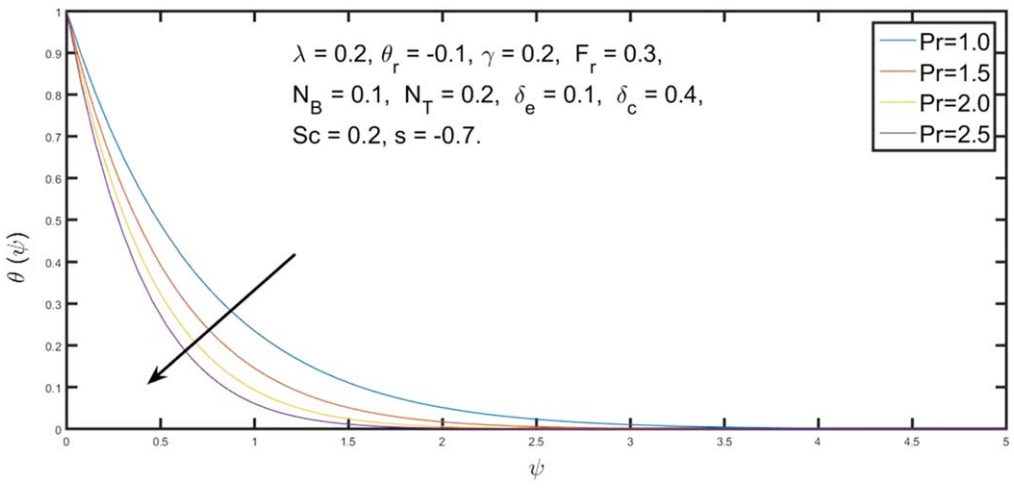

Figure 7. Effect of Pr on $\theta(\psi)$.

viscosity is directly proportional to the cohesive and adhesive forces. With an increase in the cohesive and adhesive forces, the resistance of the liquid rises because the density of the molecules is also increased.

Figure 7 reveals that the energy field and thermal layer thickness decrease with the emerging Prandtl number, Pr. The Prandtl number is inversely proportional to the temperature diffusivity and thus an escalation in Pr yields a lower

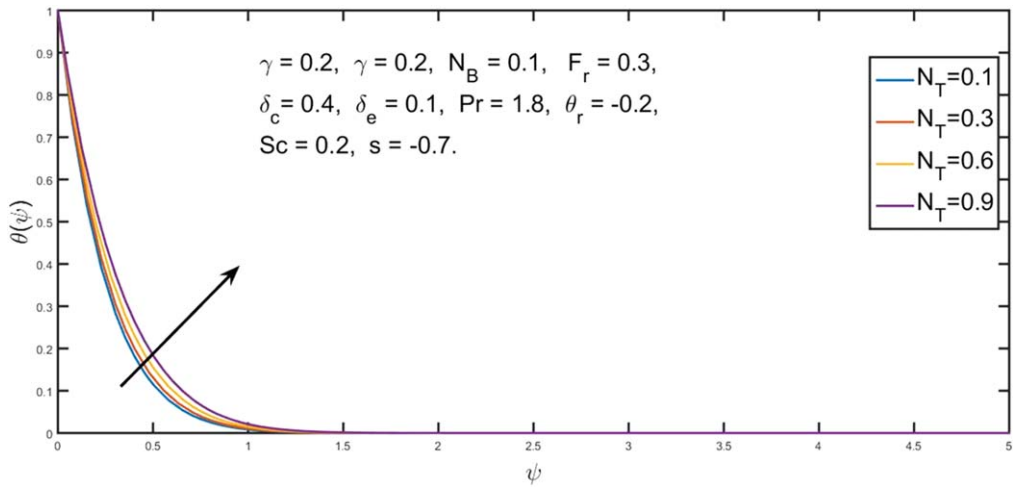

Figure 8. Effect of N_T on $\theta(\psi)$.

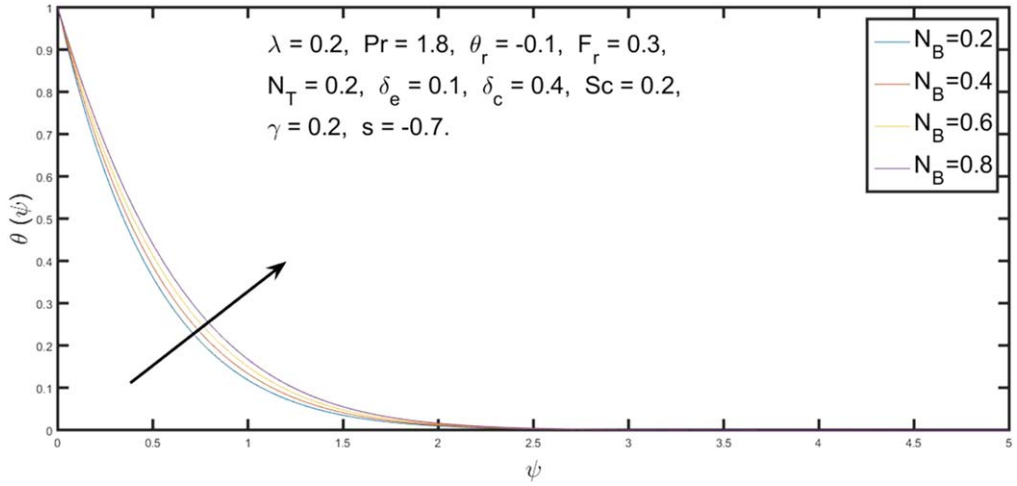

Figure 9. Effect of N_B on $\theta(\psi)$.

temperature diffusivity. If the heat diffusivity is lower than the momentum diffusivity then the distance the fluid will move to fully develop the velocity boundary layer is less compared to the distance moved for the thermal boundary layer to fully develop, causing a smaller entrance region for the velocity layer compared to the entrance region for the thermal boundary layer. Weaker heat diffusivity generates senility in the thermal field and related thermal layer thickness. Figure 8 shows the behavior of the thermophoresis parameter N_T on the energy profile. It reveals that greater values of N_T cause an increase in the thermal profile and thermal layer thickness. Interpretation beyond this accession is that exceeding values of N_T generate an energetic force. The vigorous force allows the agitation of nanoparticles departs in the region of colder liquid which proceeds a vigorous thermal profile. Figure 9 shows the importance of the Brownian movement parameter N_B relative to the energy profile. Acceleration in N_B yields an abnormal flow of liquid molecules, thus the kinetic energy of molecules rises and exceeds the thermal layer thickness. Figure 10 shows that the energy profile and thermal layer thickness decrease when we increase the heat relaxation time parameter δ_e. For high values of δ_e, liquid particles take a longer time to deport the heat to adjacent particles, which results in a lower energy distribution and thermal boundary layer.

Figure 11 shows that a higher Schmidt number, Sc, produces a diminution in the nanoparticle volume fraction distribution, as the Schmidt number is inversely related to Brownian diffusivity. An accession in Sc generates poor Brownian diffusivity. This state causes a decline in the nanoparticle volume fraction distribution and thinner solutal boundary layer. Figure 12 shows the effects of the Brownian motion parameter N_B on solutal distribution. With a higher N_B, the concentration profile and boundary layer thickness dwindle as there is a rise in molecular contact. The Brownian movement N_B exploits a force to apart from the molecules in the reverse direction of the solutal gradient, thus nanoparticles come into more persistent form. The excessive Brownian

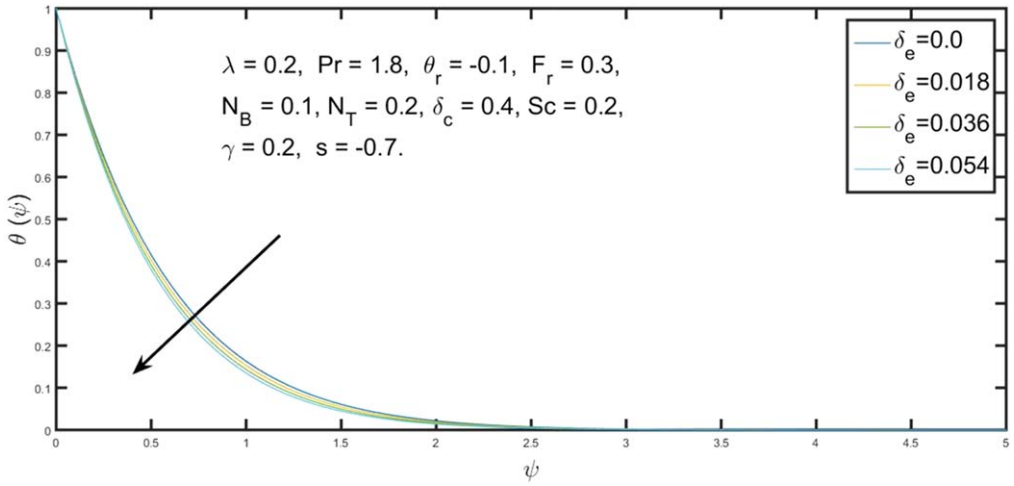

Figure 10. Effect of δ_e on $\theta(\psi)$.

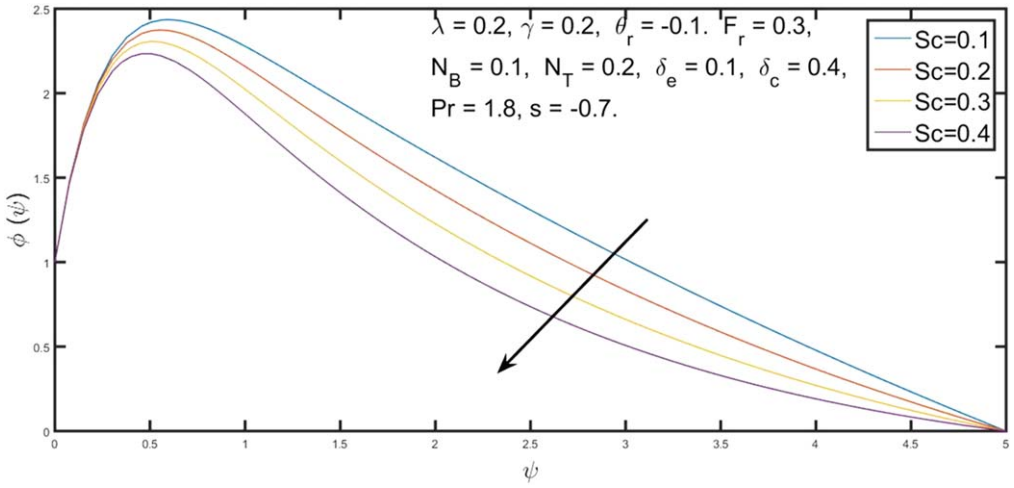

Figure 11. Effect of Sc on $\varphi(\psi)$.

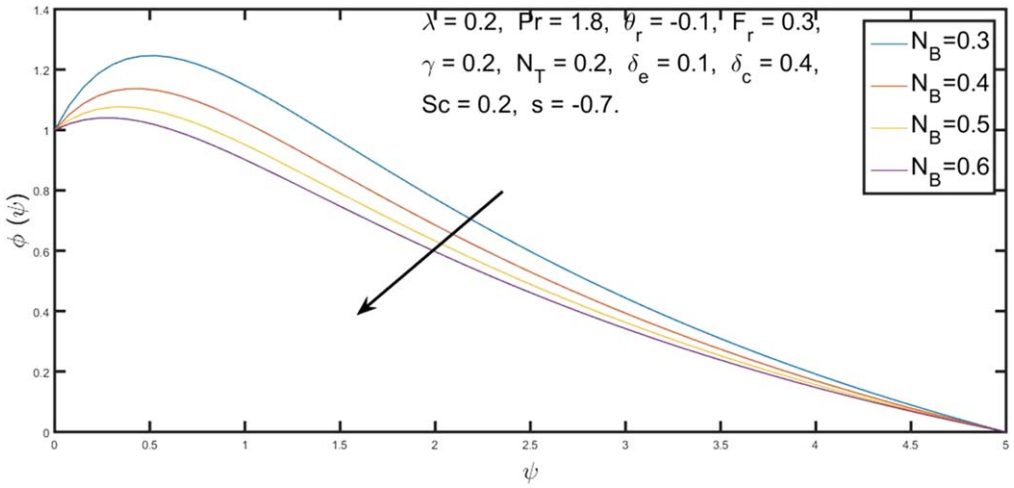

Figure 12. Effect of N_B on $\varphi(\psi)$.

force yields a lower solutal distribution. Figure 13 reveals that the boundary layer thickness and solutal gradient are extended by increasing the thermophoresis parameter N_T. The thermal conductivity of the liquid is enhanced by the nanoparticles. Thermal conductivity emerges for increasing values of N_T since increasing the thermal conductivity increases the nanoparticle volume fraction distribution. Figure 14 reveals the influence of the solutal relaxation time δ_c on the

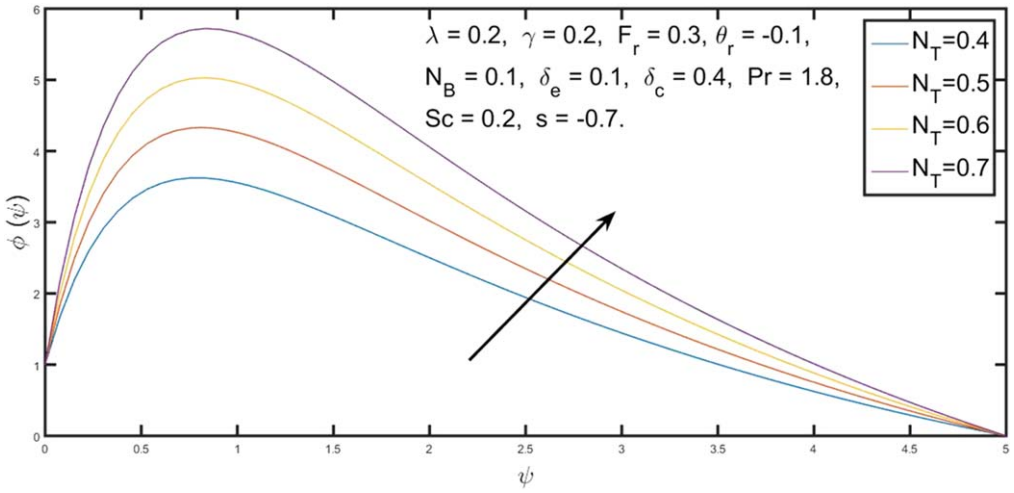

Figure 13. Effect of N_T on $\varphi(\psi)$.

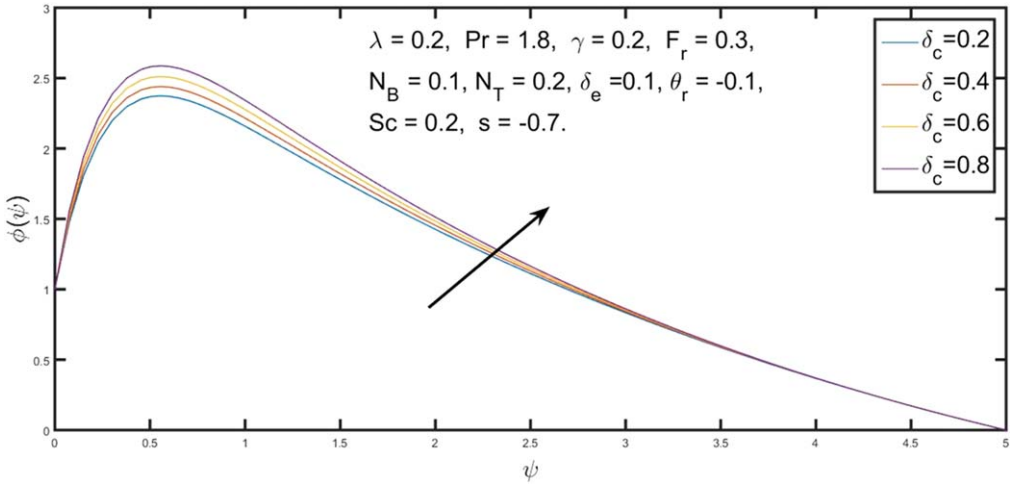

Figure 14. Effect of δ_c on $\varphi(\psi)$.

nanoparticle volume fraction distribution. For greater δ_c, the solutal distribution and boundary layer thickness decrease. When we increase δ_c, molecules need further time for mass particles to its neighboring particles, which generates a weaker nanoparticle volume fraction profile. Table 1 shows the skin friction coefficient $-Re^{\frac{1}{2}}C_g$ for miscellaneous values of θ_r, F_r, γ, s and λ. We established that the skin friction coefficient $-Re^{\frac{1}{2}}C_g$ has a decreasing trend for rising values of the variable thickness parameter θ_r, inertia coefficient F_r, porosity parameter γ, Williamson parameter λ, and suction/injection parameter s.

Concluding remarks

The aim of the current study was to address the Darcy–Forchheimer flow of Williamson nanoliquid of variable thickness restricted by a extending stretchable sheet using Cattaneo–Christov theory. The results of the investigation are summarized below:

- A diminution in velocity component $g'(\psi)$ is observed for greater values of Williamson parameter λ.
- The velocity component $g'(\psi)$ has the opposite influence via porosity parameter γ.
- A decrement is noted in the velocity distribution $g'(\psi)$ for exceeding values of inertia coefficient F_r.
- The velocity distribution $g'(\psi)$ has opposite trend through variable thickness θ_r.
- For dominating values of N_T, temperature and solutal fields emerge.
- Temperature and solutal fields dwindle with an increase in N_B.
- Temperature and solutal distributions grow with the increasing Pr number.
- Increasing the relaxation time δ_e and solutal relaxation time δ_c has the reverse effect on velocity and solutal distributions.

Table 1. Numerical values of skin friction for various values of appearing parameters.

θ_r	F_r	γ	s	λ	f″	$-Re^{\frac{1}{2}} C_g$
−0.1	0.3	0.4	0.3	0.2	−0.1648	0.0147
				0.4	−0.1640	0.0144
				0.6	−0.1524	0.0132
				0.2	−0.1231	0.0110
				0.4	−0.0990	0.0088
				0.6	−0.0986	0.0086
				0.2	−0.6229	0.0530
				0.4	−0.3845	0.0322
				0.6	−0.2064	0.0176
			0.3	0.0	−0.5552	0.0504
			0.4		−0.4721	0.0429
			0.5		−0.0318	0.0028
			0.3	0.2	−0.3857	0.0337
			0.4		−0.1937	0.0172
			0.5		−0.0137	0.0012
			0.3	0.4	−0.4166	0.0347
			0.4		−0.2744	0.0235
			0.5		−0.1338	0.0118
		0.5	0.1	0.2	−0.3074	0.0270
		0.9			−0.0782	0.0070
		0.13			−0.0170	0.0015
		0.5	0.3		−0.2929	0.0258
		0.9			−0.0858	0.0077
		0.13			−0.0133	0.0012
		0.5	0.5		−0.2667	0.0235
		0.9			−0.0305	0.0027
		0.13			−0.0075	0.0006
	0.0	0.1			−0.2343	0.0208
	0.1				−0.2324	0.0206
	0.2				−0.1665	0.0148
	0.0	0.2			−0.4891	0.0422
	0.1				−0.3280	0.0288
	0.2				−0.2188	0.0194
	0.0	0.3			−0.2551	0.0227
	0.1				−0.2551	0.0225
	0.2				−0.2061	0.0183
−1.9	0.1				−0.1779	0.0158
−0.09					−0.0666	0.0060
−0.009					−0.0271	0.0024
−1.9	0.3				−0.1146	0.0102
−0.09					−0.0740	0.0066
−0.009					−0.0427	0.0038
−1.9	0.5				−0.0969	0.0959
−0.09					−0.0769	0.0069
−0.009					−0.0325	0.0029

References

[1] Williamson R V 1929 The flow of pseudoplastic materials *J. Ind. Eng. Chem.* **21** 1108–11

[2] Malik M Y and Salahuddin T 2015 Numerical solution of MHD stagnation point flow of Williamson fluid model past a stretching cylinder *Int. J. Nonlin. Sci. Num.* **16** 161–4

[3] Ariel P D 2009 Extended homotopy perturbation method and composition of flow past a stretching sheet *Int. J. Appl. Math.* **58** 2402–9

[4] Nadeem S and Akbar N S 2007 Meccanica *Int. J. Rock Mech.* **44** 271–8

[5] Nadeem S and Akbar N S 2011 *J. Mech. Med. Biol.* **11** 941–57

[6] Dapara and Scarpi G 2007 Perturbation solution for plastic flow of non-Newtonian williamson fluid in rock features *Int. J. Rock Mech.* **44** 271

[7] Forchheimer P 1901 Wasserbewegung durch boden *Journal of Zeitschrift Ver D Ing* **45** 1782–8

[8] Muskat M 1946 The flow of homogeneous fluids through porous media *Journal of Edwards, Michigan*

[9] Pal D and Mondal H 2012 Hydromagnetic convective diffusion of species in Darcy Forchheimer porous medium with non-uniform heat source/sink and variable viscosity *Int. Commun. Heat Mass* **39** 913–7

[10] Ganesh N V, Hakeem A K A and Ganga B 2016 Darcy Forchheimer flow of hydromagnetic nanofluid over a stretching/shrinking sheet in thermally stratified porous medium with second order slip, viscous and Ohmic dissipation effects *Ain Shams Eng. J.*

[11] Singh A K, Kumar R, Singh U, Singh N P and Singh A K 2011 *Int. Commun. Heat Mass* **54** 5633

[12] Sadiq M A and Hayat T 2016 Darcy-Forchheimmer flow of magneto Maxwell liquid bounded by convectively heated sheet *Results Physics* **6** 884–90

[13] Choi S U S 1995 Enhancing thermal conductivity of fluids with nanoparticles *Proc. 1995 ASME International Mechanical Engineering Congress and Exposition* (San Francisco, USA: ASME) 231/MD 66 99–105

[14] Buongiorno J 2006 Convective transport in nanofluids *J. Heat Transfer* **128** 240–50

[15] Kuznestov A V and Nield D A 2013 The Cheng-Minkowycz problem for natural convective boundary-layer flow in porous medium saturated by a nanofluid *Int. J. Heat Mass Transfer* **65** 682–5

[16] Mustafa M, Khan J A, Hayat T and Alsaedi A 2015 Boundary layer flow of nanofluid over a nonlinear stretching sheet with convective boundary condition *IEEE Trans. Nanotechnol.* **14** 159–68

[17] Eastman J A, Choi S U S, Li S, Yu W and Thompson L J 2001 Anomalously increased effective thermal conductivities of ethylene glycol-based nanofluids containing copper nanoparticles *Appl. Phys. Lett.* **78** 718–20

[18] Salahuddin T, Malik M Y, Hussain A, Awais M, Khan I and Khan M 2017 Analysis of tangent hyperbolic nanofluid impinging on a stretching cylinder near the stagnation point *Results Physics* **17** 426–34

[19] Rehman M M, Rosca A V and Pop I 2014 Boundary layer flow of a nanofluid past a permeable exponentially shrinking/stretching surface with second order slip using Buongiornos model *Int. J. Therm. Sci.* **77** 1133–43

[20] Khan M, Malik M Y and Salahuddin T 2017 Heat generation and solar radiation effects on Carreau nanofluid over a stretching sheet with variable thickness: using coefficients improved by Cash and Carp *Results Physics* **7** 2512–9

[21] Fourier J B J 1822 Theorie analytique De La Chaleur *Journal of Paris*

[22] Fick A Ueber diffusion *Ann. Phys.* **170** 59–86

[23] Catteneo C 1948 Sulla conduzione del calore *Atti del Seminario Matematico e Fisico dell' Universita di Modena e Reggio Emilia* **3** 83–101

[24] Christov C I 2011 On frame indifferent formulation of the Maxwell-Cattaneo model of finite-speed heat conduction *Mech. Res. Commun.* **38** 77–99

[25] Straughan B 2010 Thermal convection with the Cattaneo-Christov model *Int. J. Heat Mass Transfer* **53** 95–8

[26] Waqas M, Hayat T, Farooq M, Shehzad S A and Alsaedi A 2016 Cattaneo-Christov heat flux model for flow of variable thermal conductivity generalized Burgers fluid *J. Mol. Liq.* **220** 642–8

[27] Han S, Zheng L, Li C and Zhang X 2014 Coupled flow and heat transfer in viscoelastic fluid with Cattaneo-Christov heat flux model *Appl. Math. Lett.* **68** 659–68

[28] Hayat T, Muhammad T, Alsaedi A and Ahmad B 2016 Three dimensional flow of nanofluid with Cattaneo-Christov double diffusion *Results Physics* **6** 897–903
[29] Mustafa M 2015 Cattaneo-Christov heat flux model for rotating flow and heat transfer of upper-convected Maxwell fluid *AIP Adv.* **5** 047109
[30] Khan J A, Mustafa M, Hayat T and Alseadi A 2015 Numerical study of Cattaneo-Christov heat flux model for viscoelastic flow due to an exponential stretching surface *PLoS One* **10** e0137363
[31] Tibullo V and Zampoli V 2011 A uniqueness result for the Cattaneo-Christov heat conduction model applied to incompressible fluids *Mech. Res. Commun.* **38** 77–99
[32] Li J, Zheng L and Liu L 2016 MHD viscoelastic flow and heat transfer over a vertical stretching sheet with Cattaneo-Christov heat flux effects *J. Mol. Liq.* **221** 19–25
[33] Hayat T, Qayyum S, Shehzad S A and Alsaedi A 2017 Cattaneo-Christov double diffusion model for flow of Jeffery fluid *J. Braz. Soc. Mech. Sci.* 1–17
[34] Fang T, Zhang J and Zhong Y 2012 Boundary layer flow over stretching sheet with variable thickness *Appl. Math. Comput.* **218** 7241–52
[35] Hayat T, Farooq M, Alsaedi A and Solamy F A 2015 Impact of Cattaneo-Christov heat flux in the flow over a stretching sheet with variable thickness *AIP Adv.* **5** 087159
[36] Khader M M and Megahed A M 2013 Numerical solution for boundary layer flow due to non-linear stretching sheet with variable thickness and slip velocity *Eur. Phys. J. Plus* **128** 100
[37] Nadeem S and Hussain S T 2014 Heat transfer analysis of Williamson fluid over exponentially surface *J. Appl. Math. Mech.* **35** 489–502